Direct numerical simulation of turbulence in an internally heated convective fluid layer and implications for statistical modelling

Simulation numérique directe de la turbulence dans une couche fluide avec convection naturelle et source de chaleur interne; implications pour la modélisation statistique

MARTIN WÖRNER, MICHAEL SCHMIDT and GÜNTHER GRÖTZBACH, *Forschungszentrum Karlsruhe, Institut für Reaktorsicherheit, Postfach 3640, 76021 Karlsruhe, Germany*

ABSTRACT

Direct numerical simulations (DNS) are reported for the convection in an internally heated convective fluid layer which is bounded by rigid isothermal horizontal walls at equal temperature. The simulations for a fluid Prandtl number of seven cover seven distinct internal Rayleigh numbers in the range $10^5 \le Ra_I \le 10^9$. From the numerical database the changes of convective patterns and dynamics for increasing Ra_I, i.e. increasing turbulence intensity, are analysed. To support the development and improvement of statistical turbulence models for this special type of convection, turbulence data for mean and fluctuating temperature and velocities are provided. For the simulation with $Ra_I = 10^8$ budgets of turbulence kinetic energy k and vertical turbulent heat flux $\overline{u'_3T'}$ are presented. In addition, closure assumptions commonly used in statistical turbulence models are tested against the DNS data. It is found that the turbulent diffusive transport of k and $\overline{u'_3T'}$ is strongly underestimated by standard models. The modelling of the turbulent heat fluxes by a turbulent Prandtl number approach is totally inadequate for internally heated convection. Instead, a second moment closure for $\overline{u'_iT'}$ is required.

RÉSUMÉ

Des essais de simulation directe (DNS) sont présentés pour la convection naturelle dans un fluide avec source de chaleur interne, les conditions aux limites étant des parois horizontales rigides et isothermes de même température. Les simulations, pour un nombre de Prandtl de 7, recouvrent 7 nombres de Rayleigh dans la gamme $10^5 \le Ra_I \le 10^9$. A partir de la base de données numériques, les changements de convection et de la dynamique de l'écoulement sont analysés lorsque Ra_I croît, c'est-à-dire lorsque l'intensité de turbulence croît. Afin de permettre la modélisation statistique de la turbulence pour ce type particulier de convection, des données relatives à la turbulence sont fournies pour une température et des vitesses moyennes et fluctuantes. Pour la simulation à $Ra_I = 10^8$ des bilans d'energie cinétique turbulente k, ainsi que des flux thermiques turbulents $\overline{u'_3T'}$ sont présentés. De plus, des hypothèses de fermeture généralement utilisées dans les modèles de turbulence statistique sont utilisées et comparées aux résultats de simulation directe (DNS). Il a été trouvé que k et $\overline{u'_3T'}$ sont fortement sousestimés par les modèles classiques. La modélisation des flux thermiques turbulents par l'approche d'un nombre de Prandtl turbulent est totalement inadaptée à la convection naturelle avec source de chaleur interne. Dans ce cas, une fermeture au second ordre pour $\overline{u'_iT'}$ est nécessaire.

1 Introduction

The study of heat transfer by natural convection in cavities and fluid layers with an internal energy source is of interest for several geophysical and technological systems. For example, in nuclear engineering it is of great importance for reactor safety aspects. In severe hypothetical accidents the formation of a decay-heated pool of molten core material is assumed in the lower plenum of the reactor vessel. To retain the molten core material inside the vessel by appropriate severe accident management measures, the characteristics of heat transfer from the melt pool to the walls of the reactor pressure vessel must be sufficiently well known. This has motivated many experimental and

Open for discussion till June 30, 1998.

numerical studies of the natural convection in internally heated fluids in cavities and pools of different shapes, see [22] for a literature survey.

In another szenario it is assumed that the corium cannot be contained within the lower head of the reactor pressure vessel, and a layer of core melt forms in the lower part of the containment. In this context, the behaviour of a large plane horizontal fluid layer with volumetric energy source is of interest. Such a configuration is in particular suited to study fundamental and general features of natural convection with an internal heat source, since geometry dependent artifacts and flow phenomena which are always present in pool type containers are avoided.

Considering the convection in a large horizontal fluid layer with height $\hat{D}$ and heat generation rate $\hat{q}_v$, the important dimensionless groups which characterize the physical problem are the internal Rayleigh number $Ra_I = \hat{g}\hat{\beta}\hat{q}_v\hat{D}^5/(\hat{\nu}\hat{\kappa}\hat{\lambda})$, the Prandtl number $Pr = \hat{\nu}/\hat{\kappa}$ and the Damköhler number $Da = \hat{q}_v\hat{D}^2/(\hat{\lambda}\Delta\hat{T}_{max})$. Here, $\hat{g}$ = gravity, $\hat{\beta}$ = thermal expansion coefficient, $\hat{\nu}$ = kinematic viscosity, $\hat{\kappa}$ = thermal diffusivity, $\hat{\lambda}$ = thermal conductivity, $\Delta\hat{T}_{max}$ is the maximum temperature difference across the layer, and $\hat{\phi}$ indicates a dimensional quantity.

In literature (see [2,20] for a detailed review), results are reported mainly for two different types of thermal boundary conditions at the rigid horizontal walls. In the first more common case, the upper wall is isothermal while the lower one is adiabatic or heated. For results of theoretical, experimental and (two-dimensional) numerical investigations see [3,4,24,27], [13,14,16,19,28,33], and [7,32,34], respectively. The present paper is related to the second type of thermal boundary conditions, where the top and bottom walls are isothermal and at the same temperature. A stability analysis yields a critical Rayleigh number of $Ra_{I,c} = 37{,}325$, above which convective motion starts [31]. In experiments [11,12,17,23], where water is commonly used as working fluid and the internal energy source is simulated by Joulean heating, Rayleigh numbers up to 10^{12} have been achieved.

For reactor applications, where the Rayleigh number can attain even as high values as 10^{16}, experimental studies are supported by numerical ones in which engineering computer codes are applied. In such codes turbulent momentum and heat transfer are modelled by empirical statistical turbulence models. Therefore, the quality of the numerical results strongly depends on the reliability of the turbulence models for this special type of convection. Dinh and Nourgaliev [5] use a standard low-Reynolds-number k-ε-Pr_t model to recalculate experiments of natural convection in fluids with an internal energy source. They find that this model fails to describe the turbulent natural convection heat transfer regimes of interest. Though they propose several phenomenological corrections for the k-ε-Pr_t model, they conclude that for the development of improved turbulence models detailed data of turbulence for this type of convection is required. Unfortunately, with the exception of [14], where results for velocity and temperature fluctuations are given, no systematic experimental study on turbulence data for this type of flow exists. This is because the main objective of the respective experiments was the measurement of Nusselt numbers and the determination of integral heat transfer relations.

Since experimental turbulence data are very scarce, fundamental numerical studies have been performed to provide the desired detailed information. Two-dimensional simulations are reported in [6,12,22] for Rayleigh numbers up to 10^9, 10^8, and 10^{12}, respectively. Grötzbach [8,9,10] performed direct numerical simulations (DNS) in a three-dimensional layer. Applying periodic boundary conditions in both horizontal directions, he computed Rayleigh numbers up to $4 \cdot 10^6$. Besides presenting detailed data about turbulent velocity and temperature fields, he also analysed closure assumptions used in statistical turbulence models. Recently, in [29] the large-eddy simulation method has been used to investigate the internally heated convection at a Rayleigh number of $Ra_I = 1.5 \cdot 10^{10}$.

The objective of the present paper is to use the direct numerical simulation method to provide a turbulence database for natural convection in a horizontal fluid layer with internal heat source. We

consider convection with Rayleigh numbers in the range $10^5 \leq Ra_I \leq 10^9$. The highest Rayleigh number 10^9 is about 26,800 times the critical one, whereas in the direct numerical simulation in [10] the value $4 \cdot 10^6$ is about 107 times $Ra_{I,c}$. Thus, the new results are of much greater relevance with respect to engineering applications. To allow for a direct comparison of the numerical results with experiments performed with water, a fluid Prandtl number $Pr = 7$ is considered. The Prandtl number for corium is $Pr \approx 0.1$ for metallic and $Pr \approx 0.6$ for oxidic core melts. These values are much smaller than that for water. However, the investigation of the effect of fluid Prandtl number, as studied e.g. in [22], is out of scope of the present paper. Here, we are especially interested in fundamental features of turbulence and heat transfer in natural convection with internal heat source.
In the remainder of this paper we first present the governing equations and the numerical method. As far as experimental data are available, the numerical results are compared with measurements. The DNS database is then analysed from a phenomenological point of view by investigating the patterns and dynamics of the convection. This is followed by the analysis of turbulence modelling concepts. Results are given for the transport equations for turbulence kinetic energy and vertical turbulent heat flux. Furthermore, the DNS data are used to scrutinize closure assumptions for different terms in statistical models. The paper is completed by the conclusions.

2 Mathematical and numerical model

2.1 *Governing equations*

The equations describing turbulent flow and heat transfer are the conservation equations of mass, momentum, and energy. In the present study, we apply the Boussinesq approximation and solve the equations in dimensionless form. For normalisation the channel height $\hat{D}$, the velocity $\hat{u}_0 = (\hat{g}\hat{\beta}\Delta\hat{T}_0\hat{D})^{1/2}$, the pressure $\hat{\rho}\hat{u}_0^2$, and a temperature difference $\Delta\hat{T}_0$ are used. For a meaningful normalisation of temperature the value of $\Delta\hat{T}_0$ should be close to $\Delta\hat{T}_{max}$. However, $\Delta\hat{T}_{max}$ is not known a priori for a given energy source $\hat{q}_v$. We therefore adopt the following procedure. For a certain Rayleigh number Ra_I first the corresponding Damköhler number is estimated from experimentally derived correlations $Da = f(Ra_I)$. This value $Da_0 = \hat{q}_v\hat{D}^2/(\hat{\lambda}\Delta\hat{T}_0)$ is then used to determine $\Delta\hat{T}_0$. Applying the summation convention and considering a Cartesian coordinate system, the non-dimensional governing equations are given by:

$$\frac{\partial u_j}{\partial x_j} = 0 \tag{1}$$

$$\frac{\partial u_i}{\partial t} + \frac{\partial (u_i u_j)}{\partial x_j} = -\frac{\partial p}{\partial x_i} + \frac{1}{\sqrt{Gr_0}}\frac{\partial^2 u_i}{\partial x_j \partial x_j} - \delta_{i3}(T_{ref} - T) \qquad (i = 1, 2, 3) \tag{2}$$

$$\frac{\partial T}{\partial t} + \frac{\partial (T u_j)}{\partial x_j} = \frac{1}{Pr\sqrt{Gr_0}}\left(\frac{\partial^2 T}{\partial x_j \partial x_j} + Da_0\right) \tag{3}$$

Here, $Gr_0 = Ra_I/(Pr \cdot Da_0)$ is the Grashof number resulting from scaling.
For the numerical simulations, the following boundary and initial conditions are used: No-slip conditions are applied to all velocity components at the lower and upper walls at $x_3 = 0$ and $x_3 = 1$, respectively (see Figure 1). Both walls are isothermal and at the same dimensionless temperature $T_{W,b} = T_{W,t} = 0$. In the two horizontal directions x_1 and x_2 periodic boundary conditions are imposed.

The initial condition for the velocity field is the quiescent state, i.e. all velocity components are zero. For the temperature it is meaningful to start the simulation from a mean temperature profile which is already close to that of the fully developed convection. Here, for simulations with $Ra_I \leq 10^7$ the parabolic profile of the pure conductive regime is used as initial condition. For higher Rayleigh numbers the initial vertical mean temperature profile is given by a parabola of order eight. In all cases, random temperature fluctuations with an amplitude of typically 10% of ΔT_0 are superimposed locally on the mean profile.

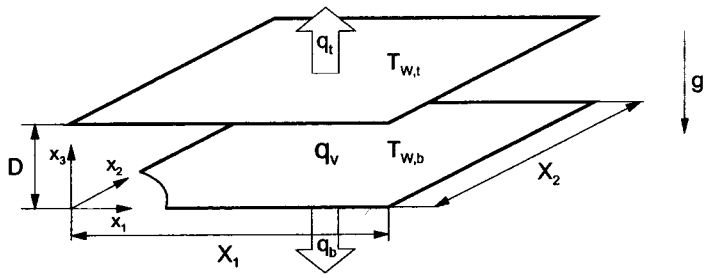

Fig. 1. Coordinate system and computational domain.

2.2 *Numerical method*

The direct numerical simulations were performed with the TURBIT code [9]. This code is based on the finite volume method, where a staggered grid is used. The convective and diffusive terms are discretized spatially by second order central finite difference approximations. In both horizontal directions the grid is equidistant, where N_1 and N_2 mesh cells of width Δx_1 and Δx_2 are used, respectively. In the vertical direction the grid spacing is non-equidistant. The mesh widths $\Delta x_3(x_3)$ are generated by a formula based on hyperbolic functions, see [1] and [26]. This ensures a smooth variation of the width of neighbouring cells.

The solution procedure for equations (1–3) is based on Chorin's projection method. It results in a Poisson equation for pressure, which is solved in a direct manner. The time advancement of equations (2) and (3) is by means of the explicit Euler-Leapfrog scheme. The accuracy is of second order for the convective terms and of first order for the diffusive terms.

In Table 1 the parameter and grid data of the simulations are listed. The mesh parameter given correspond to the last simulation of a complete series performed for each Ra_I. Starting from the initial conditions mentioned above, the solution is advanced in time on a coarse grid until, in a statistical sense, a steady state is reached. This is estimated from the temporal development of several characteristic global quantities. These are the turbulence kinetic energy, the mean temperature in the entire computational domain, and the heat fluxes at both walls. After the convection is fully developed, the local instantaneous temperature and velocity fields are interpolated to a finer grid and again integrated in time. This procedure is repeated until finally a mesh is reached which meets the spatial resolution requirements of a direct numerical simulation, to be discussed below. The procedure described drastically reduces the computation time needed to perform the simulations.

There is another criterium to check if the heat transfer is fully developed. In that case, the rate of heat generated in the fluid is the same that is removed across the lower and upper surface. The Damköhler number then just equals the sum of the Nusselt numbers at both the top and the bottom wall. In the present simulations the difference between Da and $Nu_t + Nu_b$ is very small, typically 1 to 2%. However, in the simulation for $Ra_I = 10^9$ the mean temperature in the entire domain has

not reached a steady state, but is still increasing. Additional integration in time of this simulation toward a real steady state in the mean temperature would have required immense computational costs. Therefore, the simulation has not been continued. Nevertheless, as the time trace of the turbulence kinetic energy indicates a steady state, the turbulent velocity field is fully developed. Therefore, the results for $Ra_I = 10^9$ are included in this paper.

Table 1. Parameter and grid data of the simulations.

Pr	Ra_I	$X_{1,2}$	$\Delta x_{1,2}$	$\Delta x_{3W,b}$	$\Delta x_{3,max}$	$\Delta x_{3W,t}$	N_1	N_2	N_3
	10^5	6	0.1000	0.0370	0.069	0.0320	60	60	21
	$5 \cdot 10^5$	6	0.0750	0.0250	0.064	0.0190	80	80	27
	10^6	5	0.0750	0.0250	0.064	0.0190	80	80	27
7	$5 \cdot 10^6$	5	0.0500	0.0228	0.049	0.0115	100	100	35
	10^7	5	0.0417	0.0180	0.036	0.0092	128	128	39
	10^8	4	0.0250	0.0120	0.026	0.0057	160	160	55
	10^9	3	0.0150	0.0061	0.019	0.0024	200	200	80

To ensure reliable direct numerical simulations, the smallest spatial structures of turbulence, as well as the viscous and thermal boundary layers at the top and bottom walls must be resolved by the grid. In the horizontal directions, where periodic boundary conditions are applied, the periodicity lengths X_1 and X_2 must be large enough to cover the largest macroscopic structures of the flow. We carefully checked our grids to meet these requirements, see [26]. As an example, we show in Figure 2 one-dimensional spatial energy spectra of the turbulence kinetic energy, evaluated from the DNS data for the various Rayleigh numbers at $x_3 = 0.5$. For all simulations the cut-off in this double-logarithmic representation is less than k_1^{-7}, where k_1 is the wavenumber in the x_1-direction. Thus, the mesh cells are sufficiently fine to resolve even the smallest eddies.

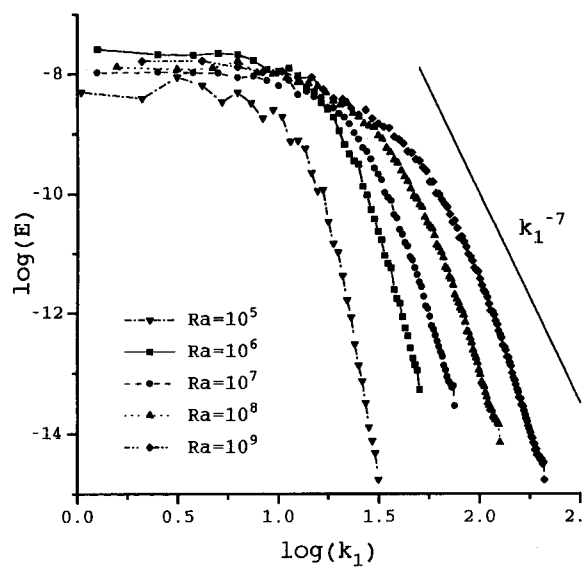

Fig. 2. One-dimensional spatial energy spectra of turbulence kinetic energy at $x_3 = 0.5$.

2.3 *Evaluation of statistical data*

For the geometry and boundary conditions used in the present direct numerical simulations, statistical data are homogeneous with respect to the horizontal directions. For this reason, the statistical evaluation of a quantity ϕ is performed by ensemble averaging of the DNS data over horizontal planes. In addition, the data are averaged over time. Typically 10 to 40 different datasets are used, each corresponding to a certain problem time. Of course, only such datasets are taken into account for which a steady state of global statistical quantities has been identified, see above. This averaging procedure results in vertical profiles and is indicated by angled brackets $\langle\phi\rangle$, whereas the overbar $\overline{\phi}$ denotes the conventional time averaging. Fluctuations with respect to $\langle\phi\rangle$ are denoted by ϕ'', and fluctuations with respect to $\overline{\phi}$ by ϕ'. For fully developed turbulent convection in a large horizontal layer, both types of averages should be equivalent, i.e. $\langle\phi\rangle = \overline{\phi}$.
In section 5, spatial derivatives need to be computed to evaluate budget terms of statistical quantities. In x_1- and x_2-direction, where the grid is equidistant, this is done by second-order central finite difference approximations. For the computation of derivatives in the vertical direction, where the grid is non-equidistant, a parabolic ansatz is used. It is based on a three-point stencil and thus is of second order, too. However, close to the walls where the spatial gradients are highest, we use a four-point stencil to ensure third-order accuracy.

3 Comparison with experiments

In this section, results of the direct numerical simulations are compared with experimental data. As discussed in the introduction, in experimental studies of internally heated convection measurements are often limited to global heat transfer parameters. While there are at least some data available for the mean temperature and the turbulent heat flux, see below, for the velocity field no experimental information at all is available in the literature. For this reason, a detailed verification of the numerical results by experiments is not possible.
In Figure 3, we compare the computed Nusselt numbers at the top and bottom wall with the experimental results of Jahn [11] and Kulacki and Goldstein [17]. The heat transfer relation of [17] (see legend in Figure 3) is obtained for $Pr = 6$ and is valid for Rayleigh numbers up to $1.2 \cdot 10^7$. In [11] the fluid Prandtl number is seven and the correlation holds up to $Ra_I = 5 \cdot 10^{10}$. From Figure 3 it is apparent that in this range of Pr the difference in fluid Prandtl number is only of small influence on the Nusselt number at top and bottom wall. At the upper wall, the numerical results agree well with both experimental heat transfer laws. However, at the lower wall there are some deviations. Especially for $Ra_I = 10^9$ the computed Nusselt number is substantially higher than in the experiments. An obvious explanation for this discrepancy may be the insufficient integration in time which does not allow for full development of the mean temperature field, as discussed above.
In Figure 4, we give a comparison of the computed vertical mean temperature profile for the simulation with $Ra_I = 10^6$ with experimental results of Kulacki and Goldstein [17]. In the upper and lower boundary layer, the agreement is very good. The same holds for the location of the maximum of the mean temperature. In the central region of the layer the DNS results show a small vertical mean temperature gradient. In contrast, in the experimental data published in [17] the core is almost isothermal. However, in subsequent unpublished experiments by the same authors, also a small increase of the mean temperature with increasing vertical position is observed in the core region [15].
For the type of boundary conditions considered here, the literature does not report any directly measured turbulence quantities which could be used for verification purposes. However, using mea-

sured temperature profiles of an experiment for $Ra_I = 8.13 \cdot 10^6$, Kulacki and Goldstein [18] deduced results for the vertical turbulent heat flux. In Figure 5, these results are compared with the turbulent heat flux evaluated from the DNS for $Ra_I = 10^7$. Though there is a difference in the Rayleigh number of about 20%, the general agreement is quite good. This is in particular true for the upper half of the layer. The differences in magnitude and in the location where the turbulent heat flux changes sign may partly be attributed to the different Rayleigh numbers.

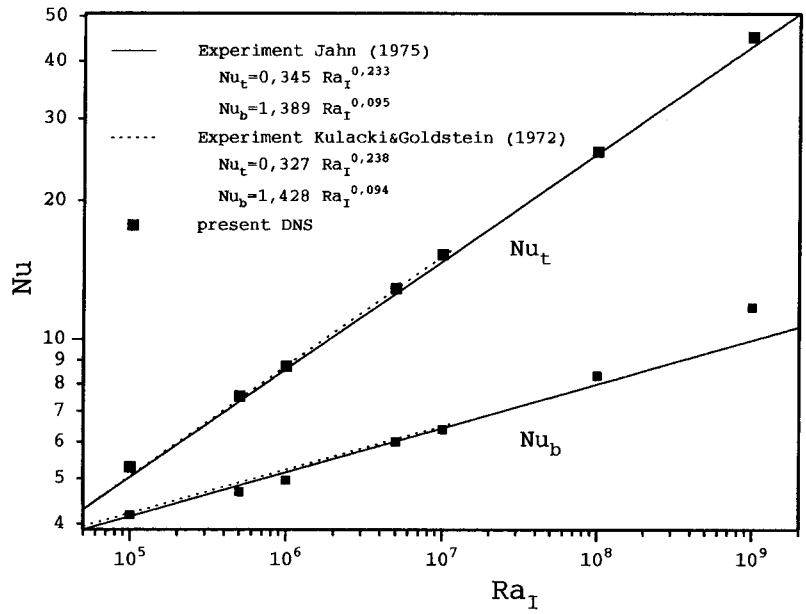

Fig. 3. Comparison of computed Nusselt numbers at the top (Nu_t) and bottom (Nu_b) wall with experimental heat transfer correlations.

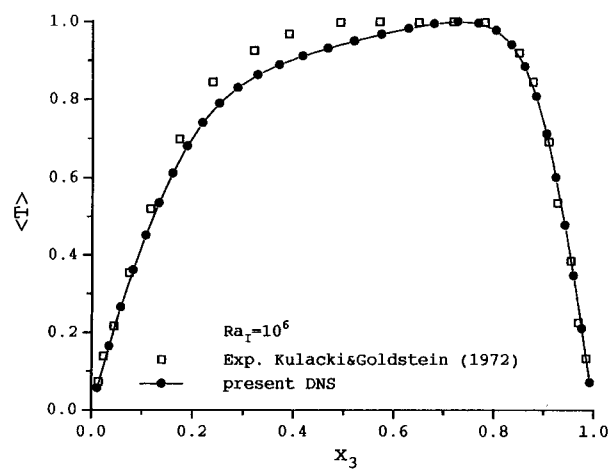

Fig. 4. Comparison of computed mean temperature with experimental results, $Ra_I = 10^6$.

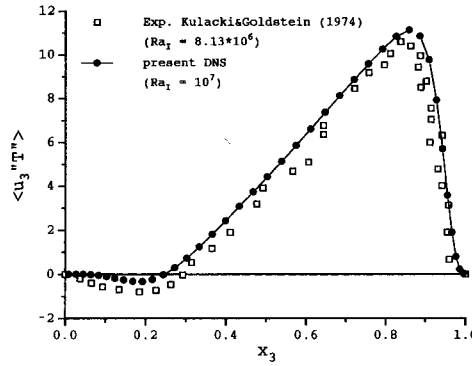

Fig. 5. Comparison of computed vertical turbulent heat flux for $Ra_I = 10^7$ with experimental results for $Ra_I = 8.13 \cdot 10^6$.

4 Patterns and dynamics of convection

To investigate the flow structures and dynamics of the convection, comprehensive visualisations of the DNS data have been performed [26]. For illustration of the relevant phenomena, in Figures 6 and 7 isolines of the instantaneous temperature in vertical and horizontal cuts through the channel are shown for various Rayleigh numbers. The dimensionless times t and the horizontal positions of the vertical cuts are arbitrary, while the vertical position of the horizontal cuts is always at the location of the maximum root-mean-square (r.m.s.) value of temperature fluctuations.

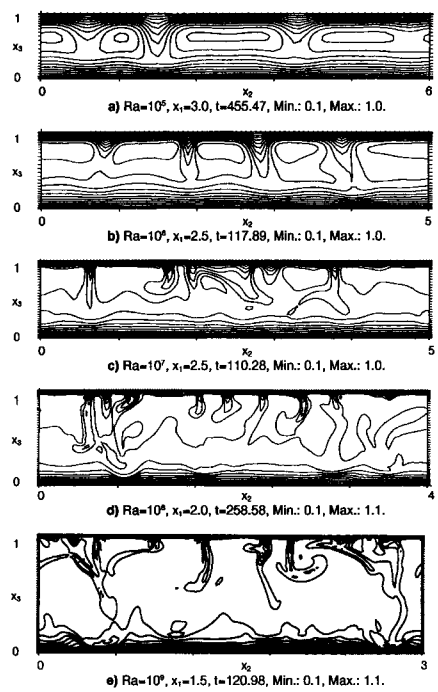

Fig. 6. Isolines of the dimensionless instantaneous temperature in vertical cuts (isoline increment = 0.1). a) $Ra_I = 10^5$, b) $Ra_I = 10^6$, c) $Ra_I = 10^7$, d) $Ra_I = 10^8$, e) $Ra_I = 10^9$.

Figures 6a and 7a show that even at the lowest Rayleigh number considered in the present study, i.e. $Ra_I = 10^5$, the flow is fully three-dimensional. The relevant convective structures are isolated cold drop-like plumes which detach from the upper isothermal wall and fall into the warmer core region. In the horizontal cut these plumes result in a pattern of concentric rings, see Figure 7a. The analysis of the temporal behaviour shows that these plumes are long-term structures. However, the convection is not stationary. There is a tendency of neighbouring plumes to merge. In larger plume-free areas emerging from this process, the thickness of the thermal boundary layer at the upper wall grows until the Rayleigh-Taylor instability develops and new plumes are formed.

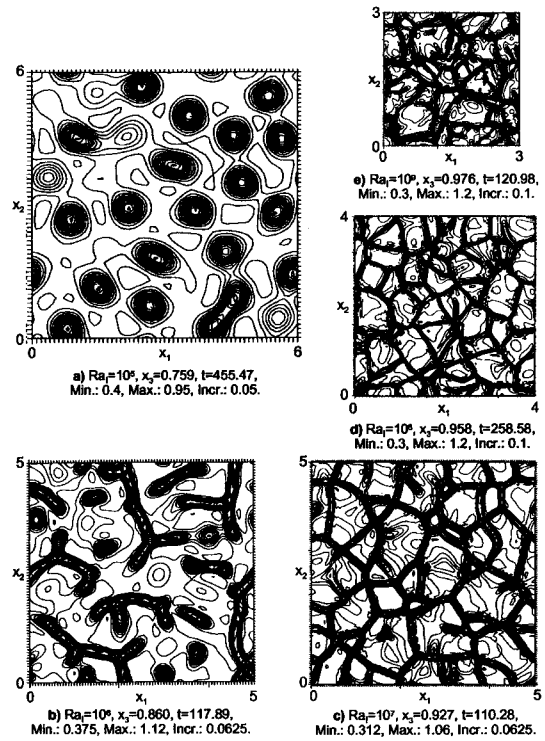

Fig. 7. Isolines of the dimensionless instantaneous temperature in horizontal cuts. a) $Ra_I = 10^5$, b) $Ra_I = 10^6$, c) $Ra_I = 10^7$, d) $Ra_I = 10^8$, e) $Ra_I = 10^9$.

In the simulation with $Ra_I = 10^6$ sheets of cold downward moving fluid are found in regions between neighbouring plumes. In the horizontal cut these vertical sheets appear as spokes, see Figure 7b. Neighbouring spokes are connected by knots, but no closed cells are formed. Besides these structures, there exist also isolated concentric ring patterns, which were already observed for $Ra_I = 10^5$ and represent falling plumes.

In the simulation for $Ra_I = 10^7$ closed irregular cells are formed by neighbouring spoke patterns in the horizontal cut, see Figure 7c. In the vertical sheets, which represent the borders of the cells, the fluid is falling fast while in the inner region of the cells the motion is upward and slow. In the temporal development of the convection, small cells contract and finally disappear. Within large cells new plumes are generated due to the Rayleigh-Taylor instability. They cause new sheets to form, which eventually divide the large cell into two or more smaller ones.

While at Rayleigh numbers below $Ra_I = 10^7$ plumes and sheets are always in connection with the boundary layer at the upper wall, at $Ra_I = 10^8$ in the core region portions of fluid may separate from the plumes or sheets, see Figure 6d. At $Ra_I = 10^9$ these mushroom-like structures of high kinetic energy deeply penetrate into the boundary layer at the lower wall, see Figure 6e.

From comparison of Figures 7c, 7d, and 7e we find that the macroscopic length scale of the irregular cells continuously decreases with increasing Rayleigh number. For this reason, in the present simulations the periodicity lengths X_1 and X_2 could be reduced with increasing Ra_I in order to save computation time without loss of relevant physical information.

A more complete representation of the structures and an impression of the dynamical phenomema occuring in an internally heated fluid layer at $Ra_I = 10^8$ is given by Figure 8, showing the instantaneous temperature field in one vertical and four horizontal cuts at different vertical positions. Cold plumes form in the unstably stratified thermal boundary layer at the upper wall. They detach and enter the warmer, almost isothermal central region of the layer. However, only few plumes of high kinetic energy reach the stably stratified thermal boundary layer at the lower wall. Therefore, the irregular cell pattern is only found in and near the upper thermal boundary layer.

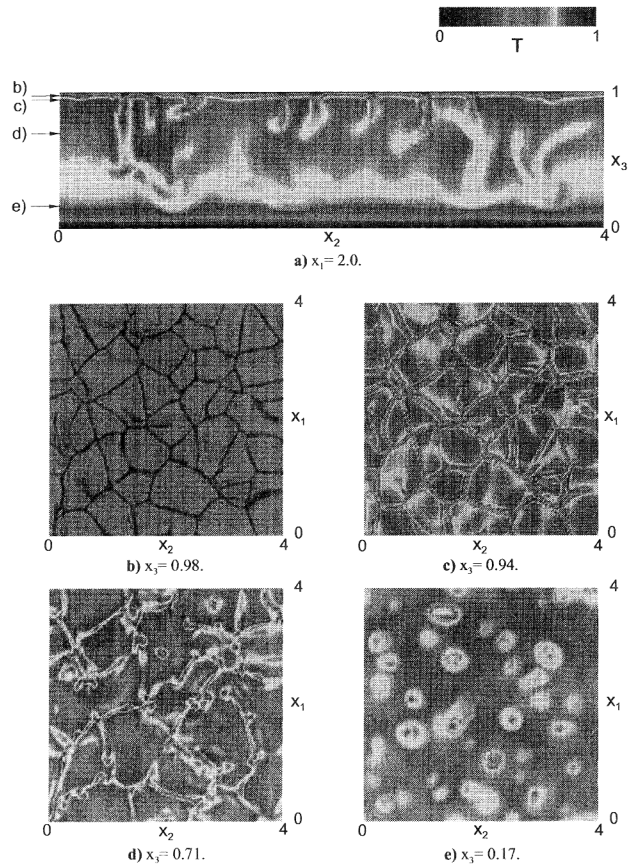

Fig. 8. Cuts through the dimensionless instantaneous temperature field for $Ra_I = 10^8$ at different positions, $t = 258.58$. a) vertical cut, b)–e) horizontal cuts.

The structures and dynamics of the convection described compare quite well with the observations by experimentalists [11,17]. The decrease of the macroscopic wavelength of the irregular cells with increasing Rayleigh number, found in the present simulations, was previously observed in all experiments as well as in direct numerical simulations [9].

5 Analysis of turbulence modelling concepts

The main objective of the present study is to provide reliable data of turbulence and to use them to test, to validate, and to improve statistical turbulence models for this special type of convection. In the following, we first give results for mean and fluctuating quantities for the various Rayleigh numbers. Subsequently, the DNS results are used to analyse budgets of the turbulence kinetic energy k and the vertical turbulent heat flux $\overline{u'_3T'}$. In addition, we test model assumptions which are commonly used for closure of various terms in standard statistical turbulence models. For these investigations, instead of using the DNS results of the highest Rayleigh number, i.e. $Ra_l = 10^9$, the simulation for $Ra_l = 10^8$ is selected for the reasons mentioned in section 2 and 3. While the convection at $Ra_l = 10^8$ is really turbulent, the turbulence Reynolds number $Re_t = k^2/(\nu\varepsilon)$ and the turbulence Peclet number $Pe_t = k^2/(\kappa\varepsilon)$ nevertheless are rather low, i.e. $Re_t \approx 4$ and $Pe_t \approx 30$.
For evaluation of statistical quantities in the following it is always assumed that the ensemble averaging procedure described in section 2.3 and the conventional time averaging, used in the statistical description of turbulence, are equivalent. Thus, for analysis of the budgets of k and $\overline{u'_3T'}$ by the DNS data all correlations of the form $\overline{\phi'\psi'}$ (or of similar type, respectively) are replaced by $\langle\phi''\psi''\rangle$. The same applies, when the performance of model assumptions for individual closure terms is tested against the DNS data.

5.1 *Statistics of the temperature and velocity fields*

In this subsection we present statistical results for the temperature and velocity fields at the different Rayleigh numbers. These results are of interest for several reasons. First, they provide insight how important statistical quantities change when the Rayleigh number and thus the turbulence intensity is increased. Second, they provide a database of turbulence which can be used to test the performance of engineering computer codes for the convection in an internally heated fluid layer. Furthermore, in common higher order statistical turbulence models closure assumptions are often based on the mean and r.m.s. values of the temperature or the velocity field. Thus, the results presented provide valuable information needed for the development and testing of improved turbulence models.
To allow for a reasonable comparison of the vertical mean temperature profiles for the different Rayleigh numbers, in Figure 9 the maximum temperature difference across the channel is normalized to $\Delta T_{max} = 1$. For $Ra_l = 10^5$ the profile of $\langle T\rangle$ differs only slightly from the parabolic one of the pure conduction regime. With increasing Rayleigh number two distinct thermal boundary layers of different thicknesses develop. The one at the top wall is thinner with thermally unstable stratification, while the thicker one at the lower wall has a thermally stable stratification. With increasing Rayleigh number the boundary layer thicknesses decrease, and in the core region of the flow the vertical gradient of the mean temperature becomes smaller and smaller. At $Ra_l = 10^9$ the profile of $\langle T\rangle$ is uniform over a broad region of the core, and thus the fluid is almost isothermal.

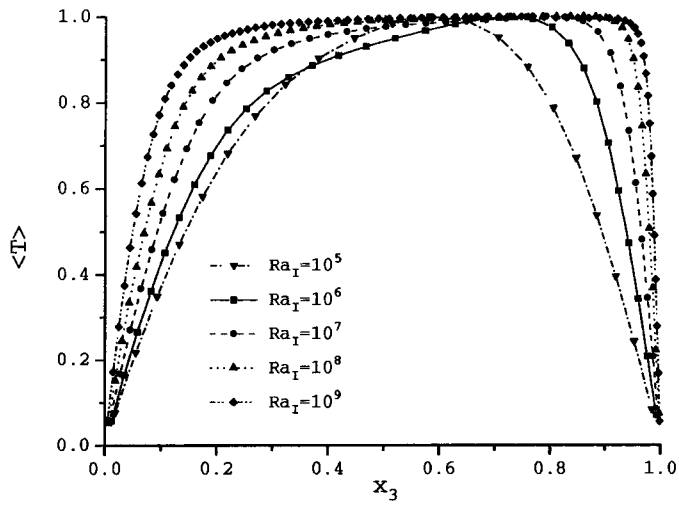

Fig. 9. Vertical profile of the mean temperature for different Rayleigh numbers.

The vertical profiles of the root-mean-square value of temperature fluctuations in Figure 10 show an absolute maximum at the edge of the thermal boundary layer at the upper wall, and a relative maximum at that of the lower wall. With increasing Ra_I the locations of both maxima shift towards the walls, so that two distinct peaks appear in the vertical profile of T_{rms}. The maximum value of T_{rms} depends only weakly on Ra_I and is always about 15% of ΔT_{max}. However, the magnitude of the relative maximum near the lower wall increases with increasing Ra_I.

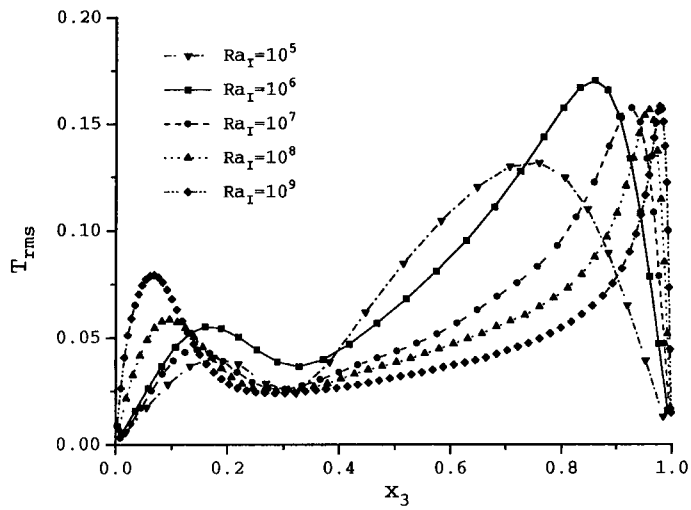

Fig. 10. Vertical profile of T_{rms} for different Rayleigh numbers.

In internally heated convection, where no horizontal mean flow through the channel is present, the ensemble averaged mean velocity $\langle \vec{u} \rangle$ is zero. The evaluated vertical profiles of $u_{1,rms}$ and of $u_{2,rms}$ are almost identical for each simulated Rayleigh number. This indicates that in each horizontal plane the horizontal velocity components are isotropic. We, therefore, present only results for $u_{1,rms}$.

With increasing Ra_I the values of $u_{1,rms}$ increase, see Figure 11. At the same time, the thicknesses of the viscous boundary layers at top and bottom wall decrease. At $Ra_I = 10^8$ and $Ra_I = 10^9$ the profile of $u_{1,rms}$ shows an almost constant value in the centre of the channel, while there is a peak at the edge of the viscous boundary layer at the upper wall.

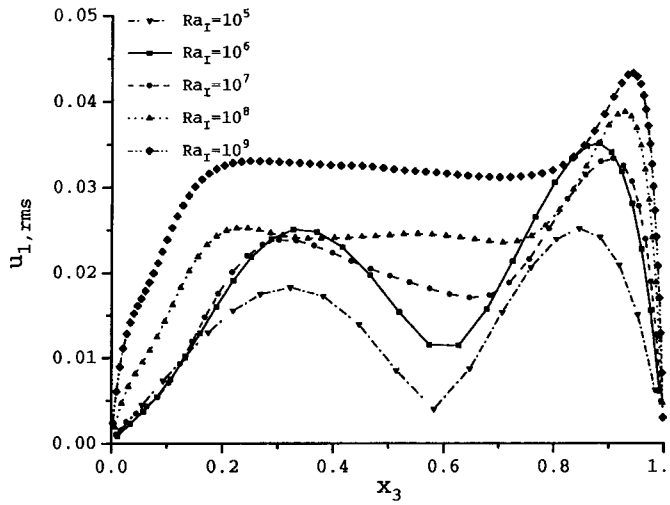

Fig. 11. Vertical profile of $u_{1,rms}$ for different Rayleigh numbers.

In the vertical profile of $u_{3,rms}$ the increase of the Rayleigh number from 10^5 to 10^8 is accompanied by a continuous increase of $u_{3,rms}$, see Figure 12. In addition, the location where $u_{3,rms}$ is maximum shifts from the middle of the layer towards the upper wall. For $Ra_I = 10^8$ and $Ra_I = 10^9$, however, the maximum of $u_{3,rms}$ takes about the same value. In accordance with the decrease of the thicknesses of the viscous boundary layers, only a broadening of the profile of $u_{3,rms}$ is observed.

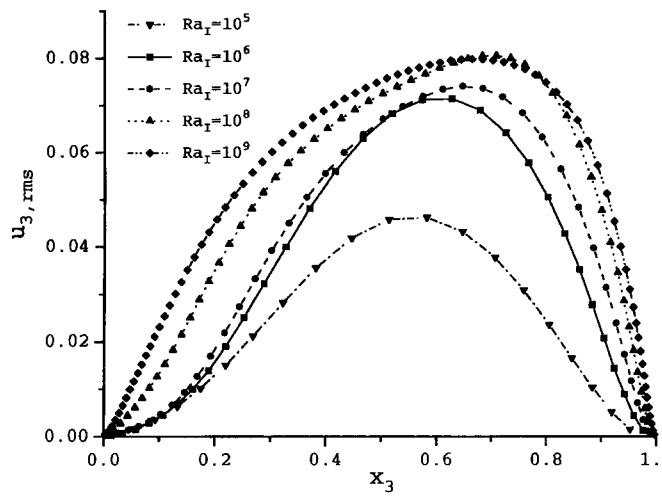

Fig. 12. Vertical profile of $u_{3,rms}$ for different Rayleigh numbers.

5.2 *Transport of turbulence kinetic energy*

In the statistical modelling of turbulence, it is a commonly used concept to determine a characteristic velocity scale of the turbulent motion by solution of a transport equation for the turbulence kinetic energy $k = {}^1/_2\overline{u'_i u'_i}$. In this subsection, we use the DNS database to analyse the budget of k and to test the performance of models for closure terms in the k-equation.

As stated above, in turbulent internally heated convection the long-time averaged mean velocities are zero. As a consequence, in the analytical transport equation for k [25] the convective transport term and the shear production term are zero. Furthermore, there is no dependence of statistical data on either horizontal direction. Therefore, the dimensionless transport equation for k reduces to

$$\frac{\partial k}{\partial t} = \underbrace{\overline{u'_3 T'}}_{G_k} \underbrace{- \frac{1}{\sqrt{Gr}} \overline{\frac{\partial u'_i}{\partial x_j} \frac{\partial u'_i}{\partial x_j}}}_{\varepsilon} \underbrace{- \frac{\partial}{\partial x_3}\left(\frac{1}{2}\overline{u'_3 u'_i u'_i} + \overline{u'_3 p'}\right)}_{D_{k,t}} + \underbrace{\frac{1}{\sqrt{Gr}} \frac{\partial^2 k}{\partial x_3^2}}_{D_{k,m}} \tag{4}$$

Here, G_k is the buoyant production/destruction, ε is the viscous dissipation, and $D_k = D_{k,t} + D_{k,m}$ is the diffusion. It consists of a turbulent ($D_{k,t}$) and a molecular ($D_{k,m}$) part. The net contribution of the diffusion term is zero since it only redistributes k across the layer.

In Figure 13, we give results for these terms, evaluated from the DNS data for $Ra_I = 10^8$. The production term G_k, which corresponds to the vertical turbulent heat flux, is zero at both walls. In the lower quarter of the channel G_k shows a small negative value, while there is a linear increase from $x_3 \approx 0.22$ to $x_3 \approx 0.9$. At $x_3 \approx 0.9$ the production G_k reaches its maximum. Except for a small region close to the lower wall, the dissipation rate ε increases monotonically with increasing x_3. From the budget of k only at two distinct vertical positions a local equilibrium between production G_k and dissipation ε is found, namely at positions where $D_k = 0$. In the predominant part of the layer diffusive transport of k is very important, as it redistributes the surplus of G_k from the centre of the layer towards the walls, where it is dissipated. The out-of-balance term $\Sigma = G_k + D_k - \varepsilon$ in Figure 13 is very small. This indicates that the time derivative in Eq. (4) is negligible and the convection is fully developed. Furthermore it confirms that the assumptions introduced above for simplification of the k-equation are valid.

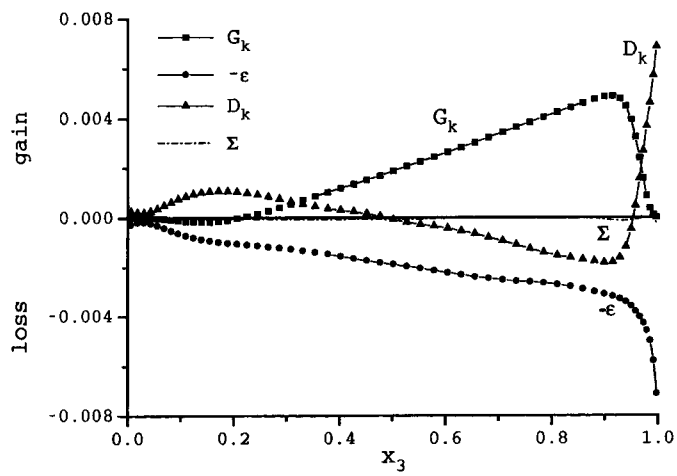

Fig. 13. Budget of turbulence kinetic energy, $Ra_I = 10^8$.

A comparison of $D_{k,t}$ and $D_{k,m}$ in Figure 14 shows that in the centre of the channel the turbulent diffusion dominates the molecular one. $D_{k,m}$ takes a very high value near the upper wall, where it balances the viscous dissipation rate. In the region $0.6 < x_3 < 0.9$ $D_{k,m}$ takes about half the value of $D_{k,t}$. While $D_{k,m}$ may be neglected at very high Rayleigh numbers, this result reveals that at low and intermediate Rayleigh numbers $D_{k,m}$ should be included in the k-equation.

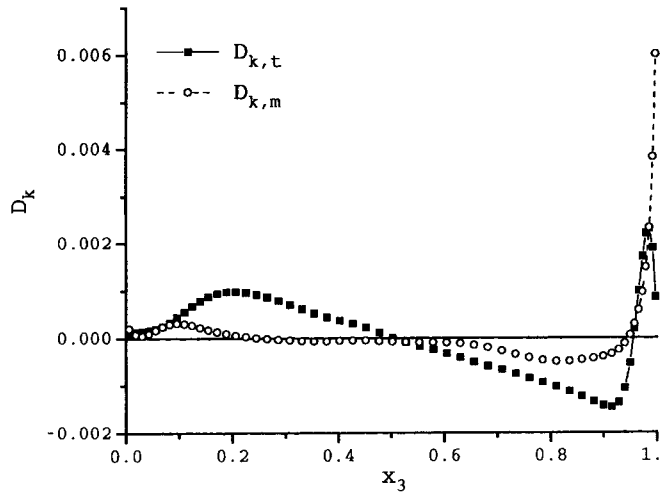

Fig. 14. Turbulent and molecular diffusion of k, $Ra_I = 10^8$.

According to Eq. (4) two correlations contribute to $D_{k,t}$. The behaviour of both the triple correlation of velocity fluctuations and the pressure-velocity correlation is dicussed in detail in [35]. There it is shown that the dominant contribution to $D_{k,t}$ is due to the triple correlation, while the pressure-velocity correlation is only of minor importance. Since both correlations appearing in $D_{k,t}$ are unknown, they have to be modelled to close the k-equation.

The standard diffusion model is based on the gradient diffusion assumption and is in analogy to the eddy diffusivity hypothesis [25]:

$$-\left(\frac{1}{2}\overline{u'_3 u'_i u'_i} + \overline{u'_3 p'}\right) \cong \frac{\nu_t}{\sigma_k}\frac{\partial k}{\partial x_3} \tag{5}$$

Here σ_k is a turbulent Prandtl number for k, usually taken to be 1. To test the performance of this model for internally heated convection, we separately evaluate both the left and right hand sides of Eq. (5) from the DNS data. As mentioned above, for this purpose the overbar is replaced by $\langle\,\rangle$ and ' by " . The eddy diffusivity ν_t in Eq. (5) is determined from

$$\nu_t = C_\mu \frac{k^2}{\varepsilon} \tag{6}$$

For the coefficient C_μ the standard value 0.09 is adopted. To achieve a better resolution of both curves in Figure 15, the scale of the ordinate for the r.h.s. of model Eq. (5) is enlarged by a factor of ten. With the exception of the range $0.7 < x_3 < 0.9$, where the turbulent diffusive transport of k is against the gradient of k, both curves compare quite well from a qualitative point of view. However,

quantitatively the diffusive transport is strongly underestimated by model (5) by about a factor of 50. The turbulent diffusive transport would thus be reasonably well predicted if the coefficient σ_k is reduced from 1 to about 0.02. Nevertheless, such a practice cannot be recommended and the present analysis indicates substantial deficiencies of the gradient diffusion model (5).

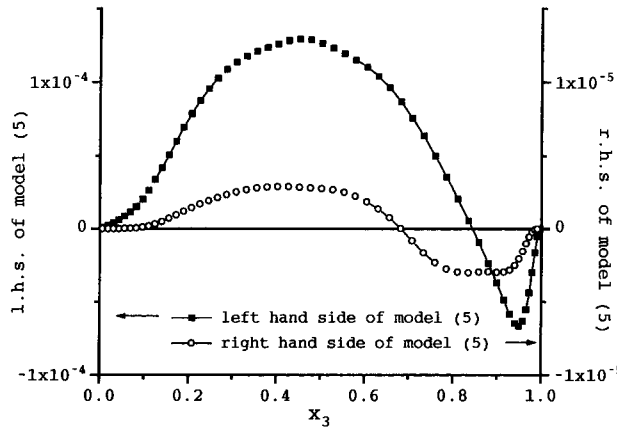

Fig. 15. Left and right hand side of model (5), $Ra_l = 10^8$.

To investigate the relevance of the discussed shortcomings of the k-ε model, we compare the results of the present analysis for $Ra_l = 10^8$ with those from previous direct numerical simulations [9,10] for $Ra_l = 4 \cdot 10^6$. Since the k-ε model is developed for high turbulence levels, one should expect that the performance of the model improves with increasing Rayleigh number. From a qualitative point of view, the budget of the k-equation at $Ra_l = 10^8$ is very similar to that reported for $Ra_l = 4 \cdot 10^6$. In [9] local equilibrium between G_k and ε is found only at two distinct vertical positions, as it also appears from the present analysis. However, with the increase of Ra_l from $4 \cdot 10^6$ to 10^8 the importance of the diffusion as redistributive term clearly has decreased. One could, therefore, expect that at very high values of Ra_l indeed a local equilibrium may exist. Considering the correlations which contribute to turbulent diffusive transport we find that the relative importance of the triple correlation as compared to the pressure correlation is substantially increased with increase of Ra_l from $4 \cdot 10^6$ to 10^8. At the same time, the region with counter-gradient diffusive transport of k has shrunk only marginally. Hence, we conclude that closure of $D_{k,t}$ by a gradient modell may be problematic even at very high Rayleigh numbers.
For statistical modelling of turbulence, an analysis of the transport equation for the dissipation ε is also of great interest. However, we do not give results here since a detailed discussion would considerably increase the size of the paper. Instead, we leave this topic to a future publication but focus in the next two subsections on the modelling of the turbulent heat fluxes.

5.3 *Concept of turbulent Prandtl number*

In natural convection the flow is driven by buoyancy forces which arise from local differences in the temperature field. Therefore, in numerical computation of such flows it is of great importance to predict the temperature field accurately. This implies that closure of the turbulent heat fluxes $\overline{u'_i T'}$ needs special care in statistical modelling of natural convection.
In simple models the turbulent heat fluxes are approximated on the basis of a gradient assumption introducing an eddy conductivity κ_t [25]:

$$\overline{u'_i T'} \cong -\kappa_t \frac{\partial \overline{T}}{\partial x_i} \tag{7}$$

Usually the concept of a turbulent Prandtl number $Pr_t = \nu_t/\kappa_t$ is used to calculate κ_t from the eddy viscosity ν_t by means of the empirically established coefficient Pr_t. To test the performance of this model for the vertical turbulent heat flux we give in Figure 16 results computed from the DNS data for the left hand and right hand side of model Eq. (7). For the analysis $\overline{u'_3 T'}$ is replaced by $\langle u''_3 T'' \rangle$ and $\overline{T}$ by $\langle T \rangle$. The eddy viscosity is again computed via Eq. (6) while for the turbulent Prandtl number the standard value 0.9 is used. From Figure 16 it becomes evident that model (7) is totally unsuited for internally heated convection. Since at high Rayleigh numbers the core region is almost isothermal and the vertical gradient of the mean temperature is very small, see Figure 9, the values of $\overline{u'_3 T'}$ predicted by model (7) are much too small. In the region $0.2 < x_3 < 0.85$ furthermore negative values of $\overline{u'_3 T'}$ are predicted while they should be positive for $x_3 > 0.2$. From the profiles of $\overline{u'_3 T'}$ in Figure 13 and from the mean temperature in Figure 9 it follows that in the entire central region of the layer a counter-gradient heat flux exists. This is not an artifact of this simulation; a counter-gradient heat flux was also found for smaller Rayleigh numbers [9]. It can also be confirmed by using the well established results for the Nusselt numbers which show that most heat is transfered upward.

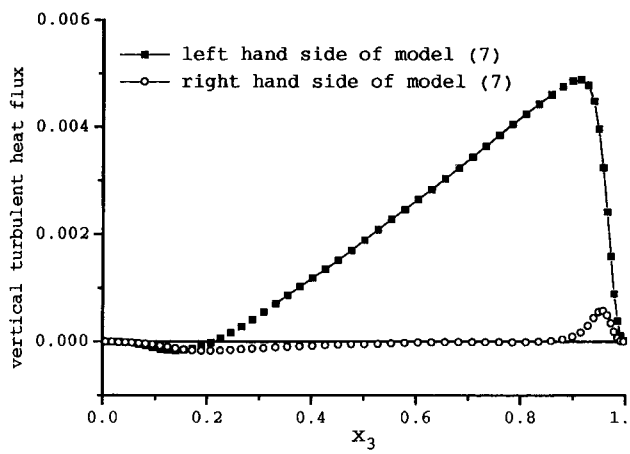

Fig. 16. Left and right hand side of model (7), $Ra_l = 10^8$.

As a consequence of these facts, the concept of a prescribed constant turbulent Prandtl number and a gradient-type relation for the closure of the turbulent heat fluxes, used in simple k-ε-Pr_t turbulence models, fails for the convection in an internally heated fluid layer. A more promising concept for modelling of the turbulent heat fluxes is to determine $\overline{u'_i T'}$ by solution of the respective transport equations. Therefore, in the next subsection we give results for the budget of the analytical transport equation for $\overline{u'_3 T'}$ and test closure assumptions for terms in this equation against the DNS data.

5.4 *Transport of turbulent heat fluxes*

With the simplifications mentioned in section 5.2, the analytical transport equation for the vertical turbulent heat flux $q = \overline{u'_3 T'}$ [25] reduces for the convection in an internally heated layer to the following non-dimensional form:

$$\frac{\partial \overline{u'_3 T'}}{\partial t} = \underbrace{-\frac{\partial}{\partial x_3}\left(\overline{u'_3 u'_3 T'} + \overline{p' T'}\right)}_{D_{q,t}} + \underbrace{\frac{1}{\sqrt{Gr}}\left(\frac{1}{Pr}\overline{u'_3 \frac{\partial T'}{\partial x_3}} + \overline{T' \frac{\partial u'_3}{\partial x_3}}\right)}_{D_{q,m}}$$

$$\underbrace{-\overline{u'^2_3}\frac{\partial \bar{T}}{\partial x_3}}_{P_q} + \underbrace{\overline{T'^2}}_{G_q} + \underbrace{\overline{p' \frac{\partial T'}{\partial x_3}}}_{\Pi_q} - \underbrace{\frac{1}{\sqrt{Gr}}\left(1 + \frac{1}{Pr}\right)\overline{\frac{\partial u'_3}{\partial x_j}\frac{\partial T'}{\partial x_j}}}_{\varepsilon_q} \tag{8}$$

In Eq. (8) $D_{q,t}$ and $D_{q,m}$ are the turbulent and molecular diffusion. Again, the net contribution of both terms is zero. P_q is the production/destruction due to the mean temperature field and G_q is the production due to buoyancy. The molecular destruction ε_q is a sink term, which is zero only in isotropic turbulence. In this case the pressure-scrambling term Π_q is the main sink of $\overline{u'_3 T'}$.

A detailed analysis of turbulent diffusive transport $D_{q,t}$ for the simulation with $Ra_I = 10^8$ is given in [35], showing that in this type of flow the dominant term in $D_{q,t}$ is the triple correlation. The pressure-temperature correlation is small except at the edge of the thermal boundary layer at the upper wall, where the profile shows a sharp peak. Considering the total diffusive transport, the turbulent part is dominant in the centre of the channel while the molecular one dominates in the boundary layers.

From Figure 17, where vertical profiles of G_q and P_q are shown, it appears that the generation of $\overline{u'_3 T'}$ is mainly due to buoyancy. At the edge of the boundary layer near the upper wall the profile of G_q exhibits a sharp peak. The generation/destruction by the mean temperature field is small, and in the lower half of the layer P_q acts as a sink term. The complete budget of $\overline{u'_3 T'}$ is shown in Figure 18 and with an enlarged scale in Figure 19. Since buoyant flows are not isotropic, it is not surprising that in internally heated convection the molecular destruction ε_q is not zero. Figures 18 and 19 even show that in the core region of the layer ε_q is the main sink term. The pressure-scrambling term Π_q is almost constant in the centre of the layer but assumes a high negative value at the upper wall. At both walls Π_q is balanced by the molecular diffusion $D_{q,m}$.

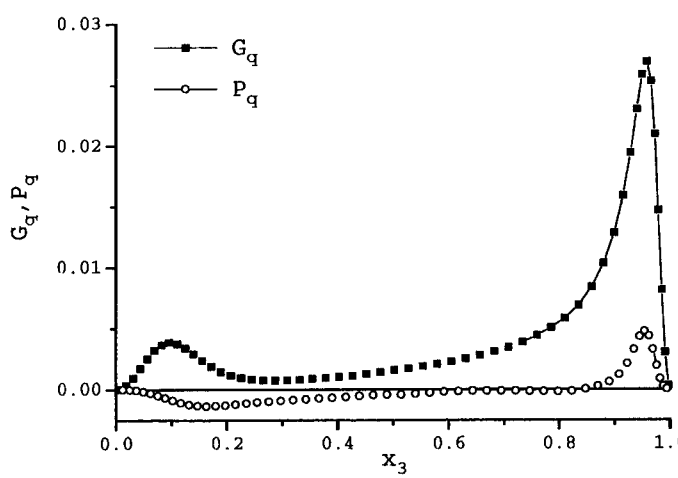

Fig. 17. Production terms G_q and P_q, $Ra_I = 10^8$.

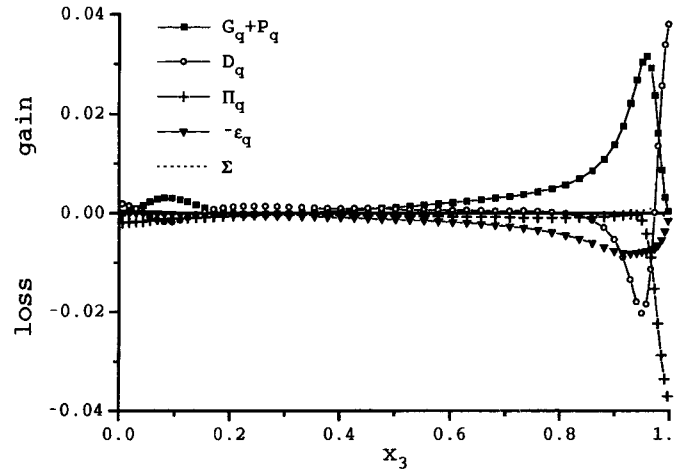

Fig. 18. Budget of vertical turbulent heat flux, $Ra_I = 10^8$.

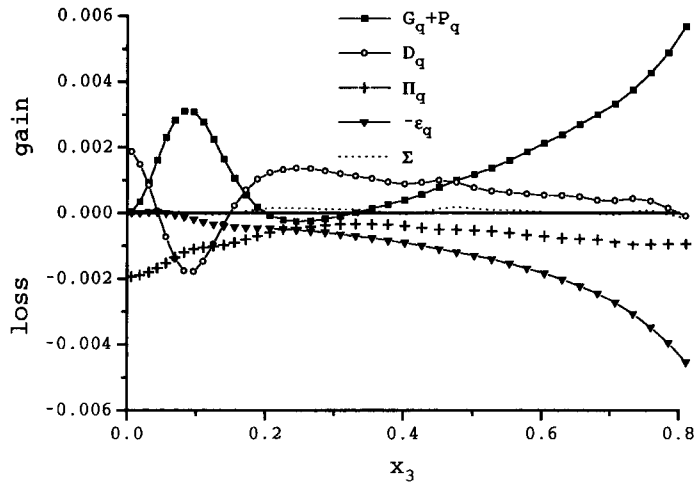

Fig. 19. Budget of vertical turbulent heat flux (enlarged scale), $Ra_I = 10^8$.

The closure terms in Eq. (8) are the buoyancy production, the molecular and turbulent diffusion, the molecular destruction, and the pressure-scrambling term. To close the buoyancy production G_q usually a separate transport equation for the temperature variance $\overline{T'^2}$ is solved [25].
Considering closures for the turbulent diffusion, we analyse a model proposed by Launder [21] for high Peclet numbers:

$$\overline{u'_3 u'_3 T'} + \overline{p'T'} \cong -C_{TD}\frac{k^2}{\varepsilon}\frac{\partial \overline{u'_3 T'}}{\partial x_3} \tag{9}$$

In Figure 20 results are given for the separately evaluated left and right hand side of model Eq. (9). For the coefficient C_{TD} the standard value 0.11 is adopted. Figure 20 reveals that from a qualitative point of view model (9) performs reasonably well for $x_3 > 0.2$. However, as was already found from the analysis

of models for the turbulent diffusion of k, the magnitude of turbulent diffusive transport is strongly underestimated by the model (compare scale of left and right ordinate in Figure 20). To account for the correct magnitude, the coefficient C_{TD} would have to be increased by about a factor of 100.

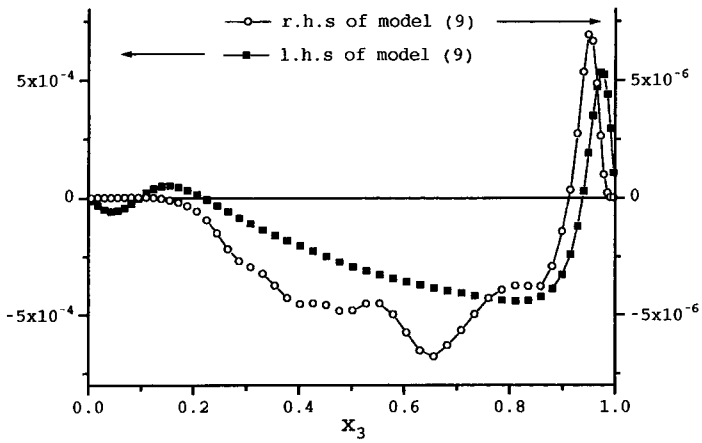

Fig. 20. Left and right hand side of model (9), $Ra_I = 10^8$.

For the pressure-scrambling term it can be shown with the aid of the Poisson equation for the pressure that Π_q has a turbulence part ($\Pi_{q,1}$), a mean-strain part ($\Pi_{q,2}$) and a buoyancy part ($\Pi_{q,3}$):

$$\Pi_q \equiv \Pi_{q,1} + \Pi_{q,2} + \Pi_{q,3} \tag{10}$$

The most widely used models for these parts are given here in dimensionless form [25]:

$$\Pi_{q,1} \cong -C_{T1}\frac{\varepsilon}{k}\overline{u'_3 T'} \tag{11}$$

$$\Pi_{q,2} \cong -C_{T2}\overline{u'_j T'}\frac{\partial \overline{u}_3}{\partial x_j} \tag{12}$$

$$\Pi_{q,3} \cong -C_{T3}\overline{T'^2} \tag{13}$$

The values commonly adopted for the coefficients are $C_{T1} = 3.0$, $C_{T2} = 0.33$ and $C_{T3} = 0.5$. Since for internally heated convection $\overline{u}_3$ is zero, $\Pi_{q,2}$ is zero, too. In Figure 21 we show vertical profiles for $\Pi_{q,1}$ and $\Pi_{q,3}$, evaluated from the DNS data for $Ra_I = 10^8$. Except the region close to the lower wall, where $\Pi_{q,1}$ is positive, the qualitative behaviour of both terms is quite similar. However, the performance of the pressure-scrambling model for the internally heated convection is poor, see Figure 22. In this figure, the term $\Pi_q = \langle p''(\partial T''/\partial x_3)\rangle$ as evaluated from the DNS data is compared with the sum of the model terms $\Pi_{q,1} + \Pi_{q,3}$. In the assessment of the model we have to distinguish between the regions inside and outside the boundary layers. While the evaluated pressure-scrambling term shows a relative and absolute minimum at the lower and the upper wall, the value predicted by the model at both walls is zero. Since model (10–13) cannot account for the damping of the vertical turbulent heat flux near the walls, it is usually extended by an appropriate wall correction term. Such terms are not considered here; thus one has to restrict the analysis to the inner part

of the channel. Figure 22 shows that outside the boundary layers, where the profile of Π_q is almost uniform, the sink rate predicted by model (10–13) is much too high.

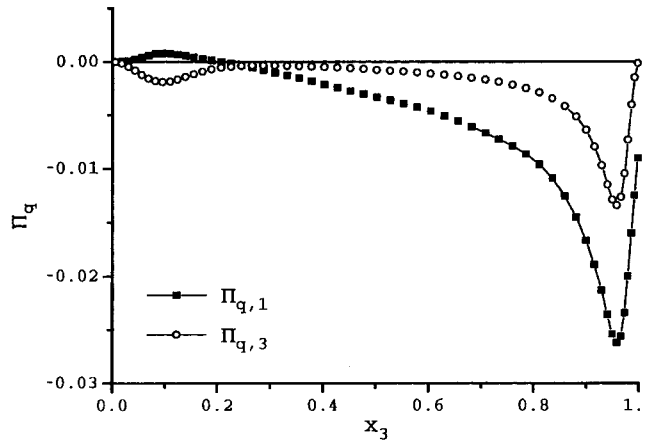

Fig. 21. Terms $\Pi_{q,1}$ and $\Pi_{q,3}$ of pressure-scrambling model, $Ra_I = 10^8$.

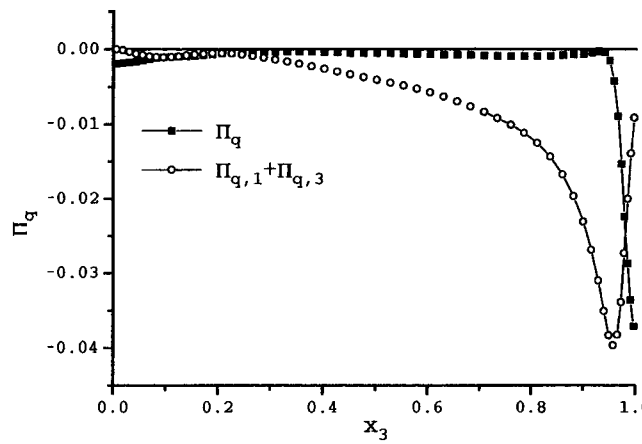

Fig. 22. Pressure-scrambling term Π_q evaluated from Eq. (8) and sum of model terms $\Pi_{q,1}$ and $\Pi_{q,3}$ from Eq. (11) and (13), $Ra_I = 10^8$.

Another closure term in Eq. (8) is the molecular destruction ε_q. The budget of $\overline{u'_3 T'}$ in Figures 18 and 19 shows that for $Ra_I = 10^8$ the main sink term is ε_q and not the pressure-scrambling term Π_q. This even holds for $Ra_I = 10^9$, though the importance of Π_q has clearly increased. Nevertheless, we conclude that in statistical modelling of internally heated convection at Rayleigh numbers of $Ra_I = 10^9$ and presumably even higher ones, the molecular destruction ε_q may not be neglected but must be modelled adequately. However, as ε_q vanishes in isotropic turbulence, in high Reynolds number models this term is usually neglected and only recently models for ε_q have been proposed in the literature [30].

6 Conclusions

In the present paper direct numerical simulations of the convection in an internally heated horizontal fluid layer are reported. The boundary conditions are periodic in both horizontal directions while

the rigid top and bottom walls are isothermal and at equal temperature. Results are given for a fluid Prandtl number of seven and various internal Rayleigh numbers in the range $10^5 \le Ra_I \le 10^9$.

From the direct numerical simulations, the patterns and dynamics of convection are investigated for the different Rayleigh numbers. While at $Ra_I = 10^5$ single cold drop-like plumes detaching from the upper wall are predominant, at $Ra_I = 10^6$ few spoke patterns appear at the edge of the upper boundary layer. At $Ra_I = 10^7$ neighbouring spokes form closed irregular cells. With a further increase of Ra_I to 10^8 and 10^9 the macroscopic length scale of the irregular cells decreases. These structures and mechanisms are the same as observed in experiments. The qualitative and quantitative verification shows that Rayleigh numbers up to 10^8 and 10^9 are now accessible by direct numerical simulations. The present simulations, therefore, represent a reliable database which can be used for analysis of statistical features of turbulence in internally fluid layers, as well as for scrutiny and validation of statistical turbulence models for this special type of convection. In the present paper detailed results are given for the mean and fluctuating temperature and velocity fields at the various Rayleigh numbers. For the simulation with $Ra_I = 10^8$ budgets of the turbulence kinetic energy k and the vertical turbulent heat flux $\overline{u'_3 T'}$ are analysed, and closure assumptions commonly used in statistical turbulence models are tested against the DNS data.

The analysis of the budget of the turbulence kinetic energy reveals that production and dissipation of k are not in local equilibrium. While the DNS data show that the redistribution of k by turbulent diffusive transport is considerable, the standard model used for closure of this term predicts much too small values. As modelling of the vertical turbulent heat flux is concerned, the simple gradient transport and turbulent Prandtl number concept totally fails to account for the counter-gradient heat transport which occurs across about 70% of the channel height. Therefore, for an adequate description of the turbulent heat transfer models have to be used which solve transport equations for the turbulent heat fluxes and which are able to allow for counter-gradient heat transport.

From analysis of the budget of $\overline{u'_3 T'}$ it appears that the main sink term is not the pressure-scrambling term but the molecular destruction. Thus, this term may not be neglected but must be modelled even at $Ra_I = 10^8$ and much higher Rayleigh numbers. For closure of the pressure-scrambling term, the standard model is found to perform poorly. As regards to the modelling of the turbulent diffusion of $\overline{u'_3 T'}$, the rate predicted by the standard model is found to be much too low.

From comparative assessment of the results for $Ra_I = 10^8$ with direct numerical simulations reported in literature for $Ra_I = 4 \cdot 10^6$ we conclude that main features of turbulence in internally heated convection, e.g. counter-gradient heat transport and counter-gradient diffusive transport of k, are still present at the substantially higher turbulence level considered here. Thus, they may persist at even higher Rayleigh numbers. For reactor applications, however, internal Rayleigh numbers up to 10^{16} can be expected and additional phenomena may occur. With today's computer power, such Rayleigh numbers are far beyond the capabilities of the direct simulation method. They can be handled only by large-eddy simulations or statistical simulations of turbulence. In this context, the present results are of interest for the development of reliable turbulence models applicable to the convection in fluids with internal energy release.

Notations

C_{T1}, C_{T2}, C_{T3}	Coefficients in model for Π_q
C_{TD}	Coefficient in model for $D_{q,t}$
C_μ	Coefficient in k-ε model
$\hat{D}$	channel height

$D_{k,m}$ molecular diffusion in k-equation
$D_{k,t}$ turbulent diffusion in k-equation
$D_{q,m}$ molecular diffusion in $\overline{u'_3T'}$ -equation
$D_{q,t}$ turbulent diffusion in $\overline{u'_3T'}$ -equation
Da Damköhler number, $\hat{q}_v\hat{D}^2/(\hat{\lambda}\Delta\hat{T}_{max})$
$\hat{g}$ gravitational acceleration
G_k buoyancy production in k-equation
G_q buoyancy production in $\overline{u'_3T'}$ -equation
Gr Grashof number, $Ra_I/(Pr \cdot Da)$
k turbulence kinetic energy, $\overline{u'_iu'_i}/2$
k_1 wavenumber in x_1-direction
N_i number of mesh cells in x_i-direction
Nu Nusselt number
p pressure
P_q production term in $\overline{u'_3T'}$ -equation
Pe_t turbulence Peclet number, $k^2/(\kappa\varepsilon)$
Pr Prandtl number, $\hat{\nu}/\hat{\kappa}$
Pr_t turbulent Prandtl number
q_i turbulent heat flux in x_i-direction, $\overline{u'_iT'}$
$\hat{q}_v$ volumetric heat source
Ra_I internal Rayleigh number, $\hat{g}\hat{\beta}\hat{q}_v\hat{D}^5/(\hat{\nu}\hat{\kappa}\hat{\lambda})$
Re_t turbulence Reynolds number, $k^2/(\nu\varepsilon)$
t time
T temperature
ΔT temperature difference
u_i velocity component in x_i-direction
$\hat{u}_0$ velocity scale, $(\hat{g}\hat{\beta}\Delta\hat{T}_0\hat{D})^{1/2}$
x_i coordinates in horizontal (i = 1,2) and vertical (i = 3) direction
Δx_i mesh width in x_i-direction
X_i periodicity length in x_i-direction (i = 1,2)

Greek

$\hat{\beta}$ coefficient of thermal expansion
δ_{ij} Kronecker delta
ε dissipation
ε_q molecular destruction in $\overline{u'_3T'}$ -equation
κ thermal diffusivity
κ_t eddy conductivity
$\hat{\lambda}$ thermal conductivity
$\hat{\nu}$ kinematic viscosity
ν_t eddy viscosity
Π_q pressure-scrambling term
$\Pi_{q,i}$ parts of Π_q, i = 1,2,3
$\hat{\rho}$ density
σ_k turbulent Prandtl number for k
ϕ,ψ general variables

Subscripts

b	bottom wall
c	critical value
k	term in k-equation
m	molecular
max	maximum
q	term in $\overline{u'_3 T'}$ -equation
ref	reference value
rms	root-mean-square value
t	top wall, turbulent
W	wall
0	initial or normalisation value

Superscripts

$\hat{\phi}$	dimensional variable
$\bar{\phi}$	time average
ϕ'	fluctuating component with respect to $\bar{\phi}$
$\langle\phi\rangle$	ensemble average over x_1-x_2-plane and time
ϕ''	fluctuating component with respect to $\langle\phi\rangle$

References

1. AGRAWAL, A.K. and PECKOVER, R.S. (1980), Nonuniform grid generation for boundary layer problems, Computer Physics Communications, 19, 171–178.
2. BAKER, L., FAW, R.E. and KULACKI, F.A. (1976), Postaccident heat removal - Part I: Heat transfer within an internally heated nonboiling liquid layer, Nuclear Science and Engineering, 61, 222–230.
3. CHEUNG, F.B. (1977), Natural convection in a volumetrically heated fluid layer at high Rayleigh numbers, Int. J. Heat Mass Transfer, 20, 499–506.
4. CHEUNG, F.B. (1980), Heat source-driven thermal convection at arbitrary Prandtl number, J. Fluid Mech., 97, 743–758.
5. DINH, T.N. and NOURGALIEV, R.R. (1997), Turbulence modelling for large volumetrically heated liquid pools, Nuclear Engineering and Design, 169, 131–150.
6. EMARA, A.A. and KULACKI, F.A. (1980), A numerical investigation of thermal convection in a heat-generating fluid layer, ASME J. Heat Transfer, 102, 531–537.
7. FAROUK, B. (1988), Turbulent thermal convection in an enclosure with internal heat generation, ASME J. Heat Transfer, 110, 126–132.
8. GRÖTZBACH, G. (1982), Direct numerical simulation of turbulent momentum and heat transfer in an internally heated fluid layer, Proc. 7th Int. Heat Transfer Conf., Munich, Germany, Vol. 2, 141–146.
9. GRÖTZBACH, G. (1987), Direct numerical and large eddy simulation of turbulent channel flows, in: "Encyclopedia of Fluid Mechanics", Ed.: N.P. Cheremisinoff, Gulf Publishing, Houston, 6, 1337–1391.
10. GRÖTZBACH, G. (1989), Turbulent heat transfer in an internally heated fluid layer, Proc. 3rd Int. Symp. on Refined Flow Modelling and Measurements, Eds.: Y. Iwasa, N. Tamai and A. Wada, Universal Academy Press, Tokyo, Japan, 267–275.
11. JAHN, M. (1975), Holographische Untersuchung der freien Konvektion in einer Kernschmelze, Dissertation, TU Hannover.
12. JAHN, M. and REINEKE, H.H. (1974): Free convection heat transfer with internal heat sources; Calculations and Measurements, 5th Int. Heat Transfer Conf., Tokyo, Japan, paper NC 2.8.
13. KIKUCHI, Y., KAWASAKI, T. and SHIOYAMA, T. (1982), Thermal convection in a horizontal fluid layer heated internally and from below, Int. J. Heat Mass Transfer, 25, 363–370.
14. KIKUCHI, Y., SHIOYAMA, T. and KAWARA, Z. (1986), Turbulent heat transport in a horizontal fluid layer heated internally and from below, Int. J. Heat Mass Transfer, 29, 451–461.
15. KULACKI, F.A. (1982), personal communication.

16. KULACKI, F.A. and EMARA, A.A. (1977), Steady and transient thermal convection in a fluid layer with uniform volumetric energy sources, J. Fluid Mech., 83, 375–395.
17. KULACKI, F.A. and GOLDSTEIN, R.J. (1972), Thermal convection in a horizontal fluid layer with uniform volumetric energy sources, J. Fluid Mech., 55, 271–287.
18. KULACKI, F.A. and GOLDSTEIN, R.J. (1974), Eddy heat transport in thermal convection with volumetric energy sources, 5th Int. Heat Transfer Conf., Tokyo, Japan, paper NC 2.6.
19. KULACKI, F.A. and NAGLE, M.E. (1975), Natural convection in a horizontal fluid layer with volumetric energy sources, ASME J. Heat Transfer, 97, 204–211.
20. KULACKI, F.A. and RICHARDS, D.E. (1985), Natural convection in plane layers and cavities with volumetric energy sources, in: "Natural Convection: Fundamentals and Applications", Eds.: S. Kakac, W. Aung and R. Viskanta, Springer, 179–255.
21. LAUNDER, B.E. (1976), Heat and Mass Transport, in: "Topics in Applied Physics", Ed.: P. Bradshaw, Springer, 12, 231–287.
22. NOURGALIEV, R.R., DINH, T.N. and SEHGAL, B.R. (1997), Effect of fluid Prandtl number on heat transfer characteristics in internally heated liquid pools with Rayleigh numbers up to 10^{12}, Nuclear Engineering and Design, 169, 165–184.
23. RALPH, J.C., MC GREEVY, R. and PECKOVER, R.S. (1976), Experiments in turbulent thermal convection driven by internal heat sources, in: "Heat transfer and turbulent buoyant convection", Eds.: D.B. Spalding and N. Agfan, 2, 587–599.
24. ROBERTS, P.H. (1967), Convection in horizontal layers with internal heat generation. Theory, J. Fluid Mech., 30, 33–49.
25. RODI, W. (1980), Turbulence models and their application in hydraulics - a state of the art review, IAHR publication, Delft.
26. SCHMIDT, M., WÖRNER, M. and GRÖTZBACH, G. (1997), Direkte numerische Simulation der Konvektion in einer Fluidschicht mit interner Wärmequelle, Forschungszentrum Karlsruhe, FZKA 5916.
27. SCHWIDERSKI, E.W. (1972), Current dependence of convection in electrolytically heated fluid layers, Physics of Fluids, 15, 1189–1196.
28. SCHWIDERSKI, E.W. and SCHWAB, H.J.A. (1971), Convection experiments with electrolytically heated fluid layers, J. Fluid Mech., 48, 703–719.
29. SEITER, C. (1995), Numerische Simulation turbulenter Auftriebsströmungen in horizontalen Kanälen, Forschungszentrum Karlsruhe, FZKA 5505.
30. SHIKAZONO, N. and KASAGI, N. (1993), Modeling Prandtl number influence on scalar transport in isotropic and sheared turbulence, Proc. 9th Symp. Turbulent Shear Flows, Kyoto, Japan, Vol. 2, 18.3.1–18.3.6.
31. SPARROW, E.M., GOLDSTEIN, R.J. and JONSSON, V.K. (1964), Thermal instability in a horizontal fluid layer: effect of boundary conditions and non-linear temperature profile, J. Fluid Mech., 18, 513–528.
32. THIRLBY, R. (1970), Convection in an internally heated layer, J. Fluid Mech., 44, 673–693.
33. TRITTON, D.J. and ZARRAGA, M.N. (1967), Convection in horizontal layers with internal heat generation. Experiments, J. Fluid Mech., 30, 21–31.
34. TVEITEREID, M. and PALM, E. (1976), Convection due to internal heat sources, J. Fluid Mech., 76, 481–499.
35. WÖRNER, M. and GRÖTZBACH, G. (1997), Pressure transport in DNS of turbulent natural convection in horizontal fluid layers, in: "Turbulence, Heat and Mass Transfer 2", Eds.: K. Hanjalic and T.W.J. Peeters, Delft University Press, 351–360 (also to appear in Int. J. Heat Fluid Flow).